

# Distinguishing Erbium Dopants in $Y_2O_3$ by Site Symmetry: *ab initio* Theory of Two Spin-photon Interfaces

Churna Bhandari,<sup>1,\*</sup> Cüneyt Şahin,<sup>2,3,\*</sup> Durga Paudyal,<sup>1,4</sup> and Michael E. Flatté<sup>3,5</sup>

<sup>1</sup>*Ames National Laboratory, Iowa State University, Ames, IA 50011, USA*

<sup>2</sup>*UNAM — National Nanotechnology Research Center and Institute of Materials Science and Nanotechnology, Bilkent University, Ankara, Turkey*

<sup>3</sup>*Department of Physics and Astronomy, University of Iowa, Iowa City, IA 52242*

<sup>4</sup>*Department of Electrical and Computer Engineering, Iowa State University, Ames, Iowa 50011, USA*

<sup>5</sup>*Department of Applied Physics, Eindhoven University of Technology, Eindhoven, The Netherlands*

We present a first-principles study of defect formation and electronic structure of erbium (Er)-doped yttria ( $Y_2O_3$ ). This is an emerging material for spin-photon interfaces in quantum information science due to the narrow linewidth optical emission from Er dopants at standard telecommunication wavelengths and their potential for quantum memories and transducers. We calculate formation energies of neutral, negatively, and positively charged Er dopants and find the charge neutral configuration to be the most stable, consistent with experiment. Of the two substitutional sites of Er for Y, the  $C_2$  (more relevant for quantum memories) and  $C_{3i}$  (more relevant for quantum transduction), we identify the former as possessing the lowest formation energy. The electronic properties are calculated using the Perdew–Burke–Ernzerhof (PBE) functional along with the Hubbard  $U$  parameter and spin-orbit coupling (SOC), which yields a  $\sim 6 \mu_B$  orbital and a  $\sim 3 \mu_B$  spin magnetic moment, and 11 electrons in the Er  $4f$  shell, confirming the formation of charge-neutral  $Er^{3+}$ . This standard density functional theory (DFT) approach underestimates the band gap of the host and lacks a first-principles justification for  $U$ . To overcome these issues we performed screened hybrid functional (HSE) calculations, including a negative  $U$  for the  $4f$  orbitals, with mixing ( $\alpha$ ) and screening ( $w$ ) parameters. These produced robust electronic features with slight modifications in the band gap and the  $4f$  splittings depending on the choice of tuning parameters. We also computed the many-particle electronic excitation energies and compared them with experimental values from photoluminescence.

## I. INTRODUCTION

In general, quantum information is processed, stored, and transmitted by employing the superposition of states of photons or matter<sup>1</sup>. Rare earth-hosted crystals are emerging as promising materials for quantum information science because at low temperatures, they exhibit sharp optical transitions and long optical and spin coherence times. The narrow transitions allow these materials to be used as quantum light-matter interfaces (often spin-photon interfaces) or to optically control the underlying quantum states<sup>1</sup>. Several examples exist of wide-band-gap oxides which, when doped with rare-earth impurities, exhibit narrow optical transitions with long coherence times and high quantum efficiency due to their partially filled  $4f$  shell<sup>2</sup>. These characteristics allow the fabrication and usage of these materials in highly efficient optical amplifiers, high-power lasers, and quantum information processors<sup>3–6</sup>. The rare earths are not limited to laser applications; these are excellent candidates for solid-state platforms for quantum engineering, including the development of quantum networks<sup>7</sup>, optical quantum memories<sup>8</sup>, photon sources<sup>9</sup>, and provide excellent hardware for quantum storage of photons<sup>10</sup>. The large band gap (5.6 eV) yttria ( $Y_2O_3$ ), isostructural to  $Er_2O_3$ , is a very promising host for rare earth dopants due to its high chemical durability, thermal stability, and other uses for optical applications<sup>9,11–15</sup>. In particular, Er is appealing as its  $4f^{11}$  electron-shell configuration  $Er^{3+}$  emits at the

standard telecommunication wavelength of  $1.54 \mu m$ <sup>16</sup>.

Rare earth-doped yttria has been experimentally investigated for many years<sup>17,18</sup>, however many fundamental features, *e.g.*, formation energies, Er-site preference, defect levels, and the band gap, are not well understood due to the absence of theoretical studies apart from a few model calculations<sup>16,19,20</sup>. Therefore, a detailed first-principles study is desirable to explore the underlying physics and electronic structure, especially due to its potential for quantum information science. Er-based quantum memories typically rely on dopant sites with inversion asymmetry; the static dipole moment allows the optical transition energy to be varied with electric field, moving the transition into and out of resonance with the hosting optical cavity. Thus a material such as  $Y_2SiO_5$  is often chosen for quantum memories. Er-based quantum transducers, however, typically prefer sites with inversion symmetry so that the ensemble linewidth is narrower and less susceptible to local inhomogeneous electric fields.  $YVO_4$ , for example, is a choice for quantum transduction with inversion-symmetry Er sites.  $Y_2O_3$  has sites of both types:  $C_2$ , which are inversion asymmetry, and  $C_{3i}$ , which are inversion symmetric. Thus an important question is which of these is most stable, and whether it is possible to tune the Fermi energy, *e.g.* by co-doping or gate voltages, to select one or the other. The implications for spin-photon interfaces are direct: it might be that Er-doped  $Y_2O_3$  is preferable for quantum memories or quantum transducers but not both.

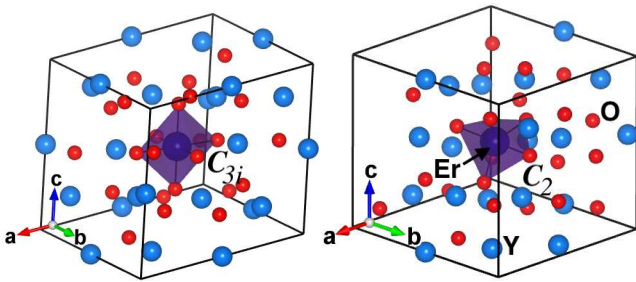


FIG. 1. Crystal structure of Er-doped  $\text{Y}_2\text{O}_3$  at  $C_{3i}$  (left) and  $C_2$  (right) sites and polyhedra. Neglecting very small ( $\sim 1\%$ ) bond length differences distorting the  $C_2$  site, the polyhedra show six nearest neighbour oxygens bonded to each Er. In the  $C_{3i}$  site, all six nearest neighbor oxygens are equidistant from Er, whereas in the  $C_2$  site they split into three subgroups each containing two oxygens. Only the Er at the  $C_{3i}$  site has inversion symmetry.

Here we study the crystal structure, defect formation energy, and electronic properties of erbium-doped yttria using improved density functional theory (DFT) methods and obtain several key results. First, from first-principles calculations, we show that the lower symmetry site (lacking inversion, more suitable for quantum memories),  $C_2$ , is energetically favorable for Er doping over the inversion-symmetric  $C_{3i}$  site (more suitable for quantum transduction). Second, we find charge neutral  $\text{Er}^{3+}$  doped in yttria has the lowest formation energy confirming its stability consistent with experimental findings. Third, we investigate the electronic band structure and provide a detailed description of the Er  $4f$  levels, laying a foundation critically needed for any future study of the many-body electronic excitation energies relevant for quantum information processing. Finally, an atomistic model for strongly coupled  $L$  and  $S$ , along with a first-principles computed spin-orbit parameter, yields first and second electronic excitation energies for the Er dopant that are in good agreement with experiment.

## II. CRYSTAL STRUCTURE AND METHODOLOGY

The primitive cell of the yttria has 40 atoms (space group  $\text{Ia}\bar{3} \# 206$ )<sup>21</sup>. For convenience, we use a conventional bixbyite supercell with 80 atoms for defect calculations. The primitive cell consists of two types of inequivalent Y sites with  $C_2(12d)$  and  $C_{3i}(4b)$  symmetry in a 3:1 ratio; the oxygen is at the  $24e$  site. To simulate the Er dopant one of the thirty-two Y atoms in the  $\text{Y}_2\text{O}_3$  cell is substituted with Er (corresponding to 3.125% Er doping). This is the lowest Er dopant concentration that we were able to simulate and it corresponds to the experimentally identified optimal 1-5% Er doping for a photoluminescence study<sup>15</sup>. Er at a  $C_{3i}$  site results in a structure symmetry  $R\bar{3}$  with space group no. 148, whereas Er at a  $C_2$  site reduces to a very low symmetry

structure  $C_2$  with space group no. 5 as shown in Fig. 1.

Two independent *ab initio* computing methods, the Vienna Simulation Package (VASP)<sup>22</sup> and Quantum Espresso (QE), were used to solve the Kohn Sham eigenvalue equations with Perdew-Burke-Ernzerhof (PBE) exchange and correlation functionals. PAW pseudopotential with full  $4f$  electrons and ultrasoft pseudopotential with frozen  $4f$  states were used in the VASP and the QE calculations, respectively. The structures were relaxed independently. Two methods were used to provide additional support for the identified very small formation energy difference for Er at the  $C_2$  site versus the  $C_{3i}$  site. The distinct formation energies appear to emerge from small bond length distortions associated with the  $C_2$  site.

Neglecting these small distortions, Er atoms occupying either of the two inequivalent Y-sites have six nearest neighbour oxygen atoms. Er at the  $C_{3i}$  site has inversion symmetry and six coordinated oxygen atoms with equal bond lengths of 2.29 Å. However, Er at the  $C_2$  site lacks inversion symmetry and the six oxygens have varying bond lengths with essentially the same average as that of the  $C_{3i}$  site: two with 2.25 Å, two with 2.28 Å, and two with 2.34 Å. We note that the different symmetry of these sites has important implications for the distinct applications of these dopants for spin-photon interfaces. The  $C_{3i}$  site has inversion symmetry and thus is nearly insensitive to electric field noise; this makes the  $C_{3i}$  site Er more useful for quantum transduction (*i.e.* microwave to optical photon transduction). Meanwhile the  $C_2$  site is sensitive to electric fields, however this can also be harnessed to achieve individual addressability through a transition energy shift with electric field, which is useful for quantum memory applications. Studies of the coupling to electric fields, or photons, are beyond the scope of this paper.

In the VASP calculations, we used Dudarev's<sup>23</sup> on-site electron-correlation for Er  $4f$  states, and the spin-orbit interaction<sup>24</sup> within the augmented plane wave (PAW) scheme<sup>25,26</sup>. Using the noncollinear spin orbit calculations including on-site electron correlation (PBE+ $U$ +SOC), both spin and orbital magnetic moments are calculated. A total energy cut-off of 500 eV for the plane-wave basis set expansion was used to achieve the self-consistent charge density and the total energy. In QE<sup>27,28</sup>, following convergence tests, we chose a uniform  $2 \times 2 \times 2$  Monkhorst-Pack  $\mathbf{k}$ -grid for reciprocal space integration and a plane wave energy cut-off of 90 Ry. The system was relaxed by a quasi-Newton algorithm until an energy convergence threshold of  $10^{-6}$  Ry and a force convergence threshold of  $10^{-4}$  Ry/Bohr were reached for self consistency. Similar convergence parameters were used in the VASP calculations.

We primarily used the HSE06 functional to study the electronic properties. The Heyd-Scuseria-Ernzerhof

(HSE) screened hybrid functional<sup>29</sup> is

$$E_{xc}^{HSE} = \alpha E_x^{HF,SR}(w) + (1 - \alpha) E_x^{PBE,SR}(w) + E_x^{PBE,LR}(w) + E_c^{PBE}, \quad (1)$$

where  $E_x^{HF,SR}$  is the short-range Hartree-Fock (HF) exchange,  $E_x^{PBE,LR}$  ( $E_x^{PBE,SR}$ ) the long-range (short-range) part of the PBE exchange functional, and  $E_c^{PBE}$  is the PBE correlation functional. The standard HSE06 approximation<sup>30,31</sup> uses HF with the mixing parameter  $\alpha = 0.25$  and the screening parameter  $w = 0.2 \text{ \AA}^{-1}$ . We further investigate the  $4f$  level splittings and band gap by tuning the HSE parameters, including the screening parameter and the value of the Hubbard  $U$  for the Er  $4f$  states. We use PBE for initial convergence and then refine with the HSE form.

Usually dopants with similar ionic radii to the atoms for which they substitute do not significantly distort the crystal structure of host materials at low doping concentrations. We notice that relaxing Er-doped yttria introduces minimum distortions in the lattice constant and atomic positions due to the similar atomic radii of Er and Y ions. The relaxed lattice constant of the pure yttria supercell is  $10.62 \text{ \AA}$ , which is in excellent agreement with experimental measurements<sup>32</sup> ( $10.60 \text{ \AA}$ ). This is a considerable improvement compared to previous studies<sup>33</sup>. Inclusion of the  $4f$  electrons yields similar lattice constants for pure and doped systems within the VASP PBE calculations. We also relaxed the structure using HSE06, which yielded  $10.58 \text{ \AA}$ ,  $\sim 1\%$  smaller than the experimental lattice constant of yttria, without any significant change in the electronic structure properties.

### III. FORMATION ENERGY

When Er is substituted in yttria, it can replace a yttrium atom at one of the two symmetrically nonequivalent sites. Since Y has a  $3+$  electronic configuration, and photoluminescence emission energies associated with  $\text{Er}^{3+}$  have been observed in doped material, we expect the neutral supercell configuration with Er in the  $3+$  state to be stable at least under some conditions. We compute the formation energy of the Er ion in yttria to verify the stable state. The formation energy of different charged configurations of the Er dopant is calculated from<sup>34</sup>

$$E_f^q(\epsilon_F) = E_{\text{tot}}^q - E_{\text{tot}}^{\text{bulk}} + E_{\text{corr}} + \sum_i n_i \mu_i \quad (2)$$

$$+ q(E_{\text{VBM}} + \epsilon_F + \Delta_{q/b}).$$

Here the first two terms stand for the total energy differences between the pristine bulk system and supercell with a defect.  $E_{\text{corr}}$  is the correction term arising from the interaction between charged supercells.  $\mu_i$  is the chemical potentials of the added (Er with negative  $n$ ) and subtracted (Y with positive  $n$ ) atoms.  $\epsilon_F$  and  $E_{\text{VBM}}$  are the

Fermi level and the valence band maximum of the pristine supercell.  $\Delta_{q/b}$  represents the potential alignment term between the charged cell and the valence band gap of the bulk supercell.

To obtain the correction term ( $E_{\text{corr}}$ ), which eliminates artifacts that arise in *ab initio* calculations with charged supercells due to the periodic boundary conditions, we have used three different methods and modified the final energies accordingly. The first method is the first-order Makov-Payne correction<sup>35</sup>. The correction term is  $q^2\alpha/2\epsilon L$  where  $q$ ,  $\epsilon$ ,  $\alpha$ , and  $L$  represent the additional charge, the dielectric constant of the host material, the lattice-dependent Madelung constant ( $\alpha = 2.8373$  for a simple cubic supercell), and the linear size of the supercell, respectively. This correction can be amended to get  $E_{\text{corr}}$  in the units of eV, such that  $E_{MP} = 14.39952\alpha q^2/2\epsilon L$  with the same definitions above, and  $L$  is in the units of  $\text{\AA}$ . We use the experimental static dielectric constant of 18.1. With the relaxed supercell size mentioned above, the first-order Makov-Payne corrections are 106.284 meV for  $+1$ , one hole or  $-1$ , one electron, and 425.138 meV for  $+2$ , two holes or  $-2$ , two electrons, charged supercells.

As a second option, we used the QE software to directly calculate the Makov-Payne correction to the total energy and obtain the same numerical results. In a third approach we employed a completely different correction scheme, the method proposed by Freysoldt, Neugebauer, and Van de Walle (FNV)<sup>36,37</sup>, which is modeled by the `sxdefectalign` software. Similar to the previous calculations, we get a charge correction of about 103 meV and 414 meV for a single and double-charged supercell, respectively. We also utilized the `sxdefectalign` software<sup>36,37</sup> to obtain the potential alignment,  $\Delta_{q/b}$ , which is usually the smallest correction term in the formation energy calculations.

We have computed formation energies for the  $C_{3i}$  site for 5 differently charged configurations:  $-2$  ( $\text{Er}^{+1}$ ),  $-1$  ( $\text{Er}^{+2}$ ),  $0$  ( $\text{Er}^{+3}$ ),  $+1$  ( $\text{Er}^{+4}$ ),  $+2$  ( $\text{Er}^{+5}$ ) of the erbium-doped yttria and include only the lowest energy  $-2$ ,  $-1$ , and  $0$  (the neutral) charged states in Fig. 2. As such, the formation energies of the positively charged Er ions are always much higher for all the Fermi levels. We find that the neutral impurity, which corresponds to the  $\text{Er}^{3+}$  state, is the most probable one for a Fermi level that is between the valence band maximum ( $0 \text{ eV}$ ) and  $2.65 \text{ eV}$ . The charge transition level (from  $0$  to  $-1$  ( $\text{Er}^{2+}$ ) shown as  $0/-1$  in the Fig. 2) appears at  $2.65 \text{ eV}$ , and another charge transition from  $-1$  to  $-2$  ( $\text{Er}^{+}$ ) occurs at a Fermi level of  $3.09 \text{ eV}$  with respect to the top of the valence band. We also calculated formation energies with the yttrium-poor (oxygen-rich) and yttrium-rich (oxygen-poor) conditions. Yttrium-poor conditions yield to lower formation energy as expected giving Er impurities a higher chance to substitute for Y atoms. For higher doping levels up to the energetic position of the bottom of the conduction band, a  $-2$  charge state is the most probable configuration, however, we are unaware that erbium has been observed in

yttria in these charged states. It is possible that for current materials the Fermi level is always near the valence band for bulk uncharged yttria, for which charge-neutral erbium +3 has the lowest formation energy. However, yttria is an excellent dielectric material<sup>38</sup> in which the Fermi level in a sufficiently thin material should be tunable by adjusting a gate voltage. Additionally, we also note that we do not find any qualitative difference in the formation energies for Er substituted in the  $C_2$  site with a slight shift in the energies to 2.64 eV and 3.05 eV for the 0/-1 and -1/-2 charge transitions, respectively.

In addition, the lower formation energy with respect to  $YO_2$ ,  $ErO_2$ , and  $Er_2O_3$  confirm the thermodynamical stability of Er doped  $Y_2O_3$  (e.g.,  $ErY_{31}O_{48}$ ). The stability conditions and the enthalpy for the host (yttria) are:

$$2\mu_Y^{Y_2O_3} + 3\mu_O^{Y_2O_3} = E_{Y_2O_3} \quad (3)$$

$$\Delta H_f = E_{Y_2O_3} - 2\mu_Y^0 - 3\mu_O^0 \quad (4)$$

where  $\Delta H_f$  and  $E_{Y_2O_3}$  are the heat of enthalpy and the chemical potential of  $Y_2O_3$ ,  $\mu_Y^{Y_2O_3}$  and  $\mu_O^{Y_2O_3}$  are the chemical potentials for yttrium and oxygen within the yttria, and  $\mu_Y^0$  and  $\mu_O^0$  are the chemical potentials for the yttrium atom and oxygen atom in bulk, respectively. We calculated the chemical potentials of a yttrium atom and an oxygen atom from the bulk four-atom conventional Y crystal and an oxygen molecule. The enthalpy of formation is -1.346 Ry (-18.313 eV) (experimentally -19.7 eV<sup>39</sup>), a negative number indicating that yttria is stable against phase separation into bulk Y and gaseous  $O_2$ . One Er substitution out of thirty-two Y should still keep the enthalpy of formation negative at least within the 8% miscibility limit provided by Ref. 40.

The chemical potentials of yttrium and oxygen are bound by the calculated values such that

$$\frac{1}{2}\Delta H_f^{Y_2O_3} + \mu_Y^0 < \mu_Y^{Y_2O_3} < \mu_Y^0 \quad (5)$$

$$\frac{1}{3}\Delta H_f^{Y_2O_3} + \mu_O^0 < \mu_O^{Y_2O_3} < \mu_O^0, \quad (6)$$

where a chemical potential closer to the heat of enthalpy ( $\Delta H_f$ ) indicates a poor condition, such as oxygen-poor or yttrium poor, and a chemical potential closer to the bulk value ( $\mu_Y^0$  and  $\mu_O^0$ ) is an oxygen or yttrium rich growth condition.

In order to incorporate Er we calculate the formation enthalpy of  $Er_2O_3$  as an example of a competing phase, as the chemical potential of the Er in yttria is bound by the enthalpy of  $Er_2O_3$  and the chemical potential of pure Er ( $\mu_{Er}^{Y_2O_3} < \mu_{Er}^0$  and  $2\mu_{Er}^{Y_2O_3} + 3\mu_O^{Y_2O_3} < \Delta H_f^{Er_2O_3}$ ) preventing the formation of  $Er_2O_3$  while keeping the same oxygen chemical potential in Eq. (5). We calculate  $\Delta H_f^{Er_2O_3}$  to be -18.806 eV for an 80-atom supercell.

Additionally, we compute the monopole correction term directly from VASP, which gives 0.14 eV for both cases when an electron or a hole is added to the supercell, which is consistent with the estimated value from the

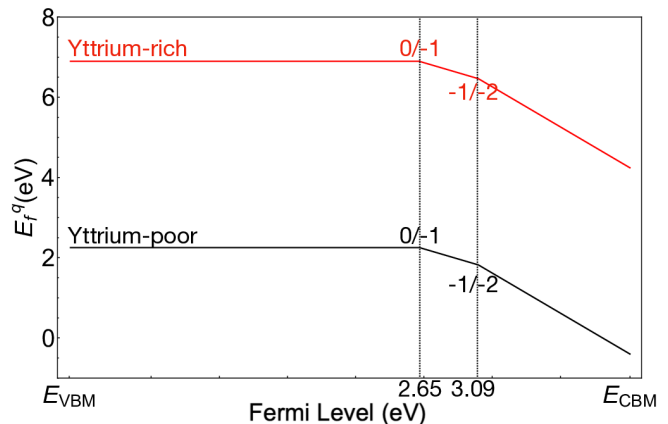


FIG. 2. Formation energies of neutral and negatively charged Er ions in  $Y_2O_3$  host as a function of the Fermi level. We select two growth conditions: yttrium-rich (red lines) and yttrium-poor (black lines) by changing the chemical potential of the Y atom in the formation energy.

first-order Makov-Payne corrections. Both VASP that includes 4f electrons as valence electrons and QE with a frozen 4f-core produce similar formation energies.

#### IV. SITE PREFERENCE AND IMPLICATIONS FOR SPIN-PHOTON INTERFACES

Er can occupy two nonequivalent sites, the  $C_2$  and  $C_{3i}$ , and the geometric ratio of  $C_2$  and  $C_{3i}$  yttrium sites is 3:1. There is a difference in the behavior and utility of the two sites for spin-photon interfaces. The  $C_2$  site possesses a static electric dipole moment due to the lack of inversion symmetry, making it more useful for quantum memories in which single ion optical transitions are moved into and out of resonance with an optical cavity using an electric field. The  $C_{3i}$  site, however, lacks that static electric dipole moment and is more useful in a narrow linewidth ensemble for quantum transduction. Experimentally electronic transitions of Er ions from both the  $C_2$  and  $C_{3i}$  sites are seen in photoluminescence<sup>15,16,19</sup>, which suggests the energy difference between the two sites is smaller than the room temperature thermal energy. Both PBE +  $U$  and HSE06 methods predict a lower energy for  $C_2$  as the site symmetry is lower than the  $C_{3i}$  site. We find a 2.6 meV lower formation energy for the  $C_2$  site compared to the  $C_{3i}$  site within PBE +  $U$  with a sensible choice of  $U_{eff} = 4$  eV. HSE06 yields a 8.3 meV (96.32 K) lower energy for the  $C_2$  site.

Although the preference energy difference is smaller than the room temperature thermal energy, most quantum devices are intended to operate at temperatures far below 1K due to the need for microwave cavities with several GHz resonant frequencies that are depleted of thermally excited photons. Thus the site energy difference

for Er far exceeds the thermal energy at temperatures of relevance for quantum devices. The Fermi energy could be positioned between that of the  $C_2$  and the  $C_{3i}$  sites by co-doping with an electron acceptor; another method would be to apply a gate voltage to deplete these electrons from the material. Yttria is a known gate electrode which can sustain substantial voltages without leakage. If the material is to be used for quantum transduction it will be important to guarantee that the  $C_{3i}$  sites are all neutral; this can be done by co-doping with electron donors or gate voltages as well. The presence of the  $C_2$  sites nearby, which will remain under these conditions, is not significantly detrimental for quantum transduction. In addition, a gate voltage could be used to shift the optical transition energies of the  $C_2$  sites far from the  $C_{3i}$  optical bandwidth relevant for quantum transduction. Thus it appears that with proper choices of co-doping and gate voltages yttria doped with erbium makes an excellent choice for quantum memories and for quantum transduction.

The VASP calculations are performed with a smaller 40 atom yttria unit cell. An independent frozen-4*f* core approximated pseudo-potential calculations with a larger 80 atom cubic cell also show similar results, confirming the independency of the cell shape and size for Er-site preference. Our calculated energy difference suggests that site-specific Er selection is possible by adjusting the temperature and changing the Fermi energy of the material with doping or electrostatic gates.

## V. ELECTRONIC STRUCTURE

### A. PBE and PBE + $U$

It is well-known that local and semi-local exchange functionals severely underestimate the band gap of semiconductors and insulators due to the self-interaction error<sup>23,41</sup>. Our VASP calculations with the PBE functional produce a band gap for yttria  $\sim 4.2$  eV, similar to previously reported results<sup>42</sup> with the same method and functional. Previously reported calculations using the orthogonalized linear combination of atomic orbitals (OLCAO) and the linear muffin-tin orbital within the atomic sphere approximation (LMTO-ASA), both with the local density functional, show a slightly higher band gap of  $\sim 4.5$  eV (at  $\Gamma$ )<sup>43,44</sup>. All these theoretical band gaps are off by  $\sim 1.6 - 1.9$  eV from experimental measurements (5.5 eV [Ref. 45], 5.6 eV [Ref. 46], and 5.9 eV [Ref. 47]) except that earlier OLCAO calculations<sup>48</sup> in the local density approximation yielded a much smaller direct band gap of 2 eV at  $\Gamma$  which the authors ascribed to a unique type of bonding ( $Y_2^{+2.16}O_3^{-1.44}$ ) in yttria.<sup>48</sup>

The PBE +  $U$  + SOC approach does better describing the band alignment as well as the splittings of strongly correlated 4*f* levels<sup>49</sup>. The electronic band structure of Er-doped yttria at the  $C_{3i}$  site (Fig. 3) is obtained with PBE +  $U$  + SOC, where  $U_{eff} = 4$  eV for the Er 4*f* orbitals. The band structure shows three localized bands

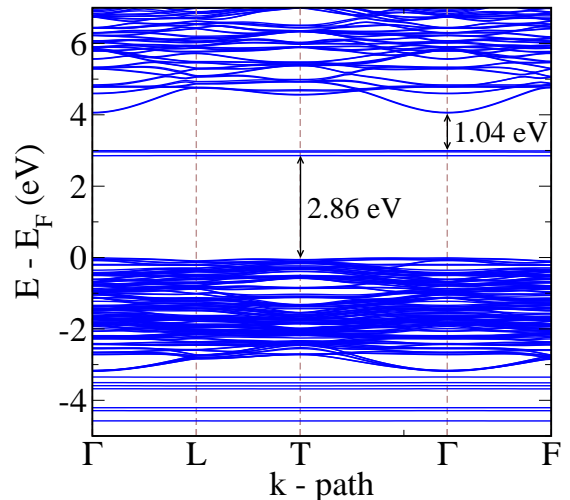


FIG. 3. PBE +  $U$  + SOC band structure of  $Y_2O_3$ , with Er-substituted into the  $C_{3i}$  site, along the high symmetry  $\mathbf{k}$ -points viz.,  $\Gamma = (0, 0, 0)$ ,  $L = (\frac{1}{2}, 0, 0)$ ,  $T = (\frac{1}{2}, -\frac{1}{2}, \frac{1}{2})$ , and  $F = (\frac{1}{2}, -\frac{1}{2}, 0)$  of the trigonal primitive unit cell with space group no. 148 ( $S_6 = C_{3i}$ ). The unoccupied 4*f* levels are split into two-manifolds, singly and doubly degenerate bands.

in the gap region (2.86 eV above the Fermi level) of the host material. The inclusion of SOC leads to additional splittings of the 4*f* levels, i.e., the threefold degenerate unoccupied states in PBE +  $U$  (see Fig. 4) split into two manifolds.

For a more detailed understanding of the electronic structure, we show the electronic density of states computed with  $U_{eff} = 4$  eV for the 4*f* states in Fig. 4 for Er doped into the  $C_{3i}$  site. The occupied Er 4*f* states split into three manifolds, with the lowest two DOS peaks substantially localized, whereas the states near the Fermi level are delocalized. The unoccupied three 4*f* levels lie 2.86 eV above the Fermi level. The Er 5*d* levels are located at 4.5 eV above the Fermi level. Our choice of  $U = 4$  eV is based on the energy difference between the occupied 4*f* and unoccupied 5*d* states, which is  $\sim 5.6$  eV, and it agrees with optical spectra<sup>15</sup>. We note that there is not much difference in the DOS for Er at the  $C_{3i}$  sites from Er at the  $C_2$  sites (not shown here). For Er at either site we find a spin magnetic moment of  $3 \mu_B$  and an orbital magnetic moment of  $\sim 6 \mu_B$  in PBE +  $U$  + SOC, which is consistent with an  $Er^{3+}$  (4*f*<sup>11</sup>) shell configuration.

Now we estimate the many body excitation energies at the atomistic level<sup>50</sup> employing the following relation,

$$E_J = \frac{\lambda}{2}[J(J+1) - L(L+1) - S(S+1)], \quad (7)$$

where  $J = L + S$  is the total angular quantum number with  $L$  the orbital and  $S$  the spin quantum numbers, and  $\lambda$  is a SOC parameter. We estimate the excitation energy between the ground state  $^4I_{15/2}$  manifold and the excited

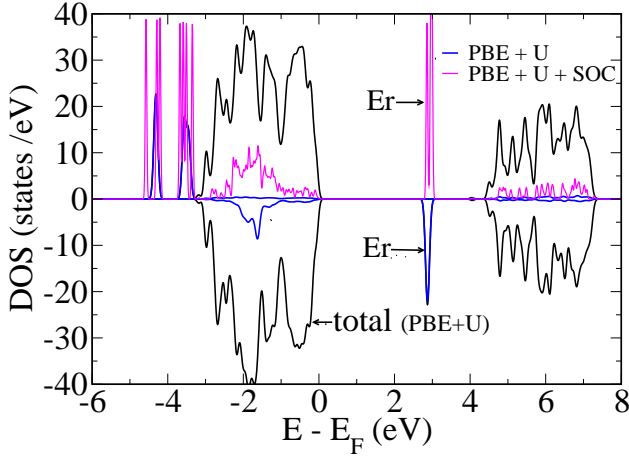


FIG. 4. Total density of states of Er-doped  $\text{Y}_2\text{O}_3$  in  $C_{3i}$  site computed with PBE +  $U$  and partial density of states (PDOS) of Er obtained with PBE +  $U$  in *blue* and PBE +  $U$  + SOC in *magenta*. Positive and negative values represent DOS for spin-up and spin-down electrons in PBE +  $U$ . The unoccupied Er 4*f* states lie in the middle of the band gap, which further split into two manifold due to SOC.

$^4I_{13/2}$  manifold,

$$\Delta E^{01} = \frac{2E_{\text{soc}}}{(J_{\text{max}} + 1)}, \quad (8)$$

using the first-principles value calculated for

$$\lambda = \frac{2E_{\text{soc}}}{J_{\text{max}}(J_{\text{max}} + 1)}, \quad (9)$$

where  $E_{\text{soc}}$  is the spin-orbit energy obtained by taking the total energy difference calculated with and without SOC, i.e.,  $E_{\text{soc}} = E_{\text{total}}(\text{PBE}+U+\text{SOC}) - E_{\text{total}}(\text{PBE}+U)$  and  $J_{\text{max}} = 15/2$ . The estimated value of  $\Delta E^{01}$  is 0.71 eV, which is in good agreement with the experimental value of 0.807 eV (1535 nm wavelength)<sup>15</sup> in photoluminescence obtained for Er-doped nanocrystals excited with 488 nm photons at room temperature. Similarly, for the ground state to the second excited state, the calculated energy is

$$\Delta E^{02} = \frac{2E_{\text{soc}}(2J_{\text{max}} - 1)}{J_{\text{max}}(J_{\text{max}} + 1)} = 1.33\text{eV}, \quad (10)$$

which is also close to the experimental value of 1.265 eV (980 nm wavelength). The discrepancy in our calculated values is reasonable due to the simplified effective atom approximation for the excitation energy.

## B. Hybrid functional

As our PBE +  $U$  + SOC calculations indicate that the Y 4*d* states are all unoccupied, the inclusion of  $U$  does not affect the band gap of the host material. For

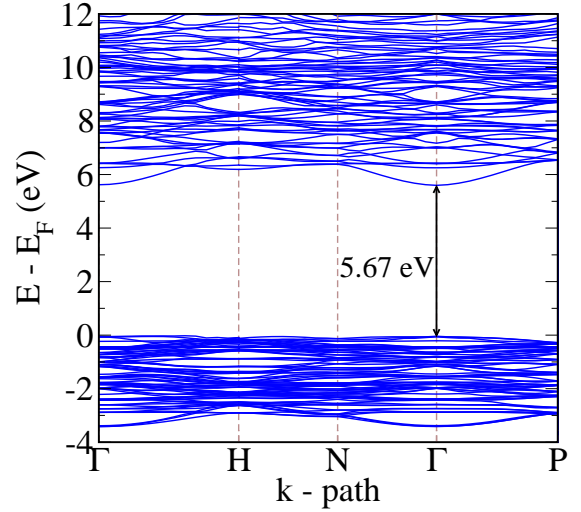


FIG. 5. HSE06 band structure of  $\text{Y}_2\text{O}_3$  along the high symmetry  $\mathbf{k}$ -points:  $\Gamma = (0, 0, 0)$ ,  $H = (\frac{1}{2}, -\frac{1}{2}, \frac{1}{2})$ ,  $N = (0, 0, \frac{1}{2})$ , and  $P = (\frac{1}{4}, \frac{1}{4}, \frac{1}{4})$  of the primitive cell space group no. 206 (Ia3).

the Er dopant the inclusion of  $U$  only affects the Er 4*f* states without altering the band gap of the host material. Whereas PBE +  $U$  produces dopant states in the gap region, it fails to predict the correct band gap of the host material. To overcome this issue, we also performed an HSE06 band structure calculations for pristine yttria as shown in Fig. 5. There is no unique choice of  $\alpha$  and  $w$  that reproduces the accurate band gap for all materials<sup>51</sup>. For instance  $\alpha = 0.25$  and  $w \sim 0.38 \text{ \AA}^{-1}$  is shown to reproduce the correct band of anatase  $\text{TiO}_2$ <sup>52</sup>, whereas  $\alpha = 0.2$  and  $w = 0.2 \text{ \AA}^{-1}$  works for rutile  $\text{TiO}_2$ <sup>53</sup>. However, for yttria the standard HSE06 calculation produces a direct band gap of 5.67 eV at  $\Gamma$ , which is in better agreement with experiment (5.6 eV) than the previously reported theoretical value<sup>42</sup> of 6 eV.

Next, we discuss our HSE results for Er-doped yttria. It is of interest to examine the effect of HSE on the Er 4*f* and 5*d* levels, which has not previously been explored to our knowledge. The only realistic comparison of our theoretical results is to the experimentally measured excitation energy between occupied 4*f* and unoccupied 5*d* states, which is  $\sim 5.8$  eV.

To check the consistency of our approach, we present the three different results by tuning the HSE parameters viz., (i) the standard HSE06 without SOC, (ii) HSE with  $\alpha = 0.2$  and  $w = 0.2 \text{ \AA}^{-1}$  and SOC, and (iii) HSE06 and SOC with  $U_{\text{eff}} = U - J = -2$  eV for Er 4*f*, as shown in Fig. 6. As expected, HSE06 improves the band gap significantly (6 eV), similar to its effect in calculations for the undoped host material. The unoccupied 4*f* levels are mixed with Y and O conduction states, which does not occur in PBE +  $U$ . The excitation energy between the occupied 4*f* and unoccupied 5*d* is  $\sim 5.87$  eV in agree-

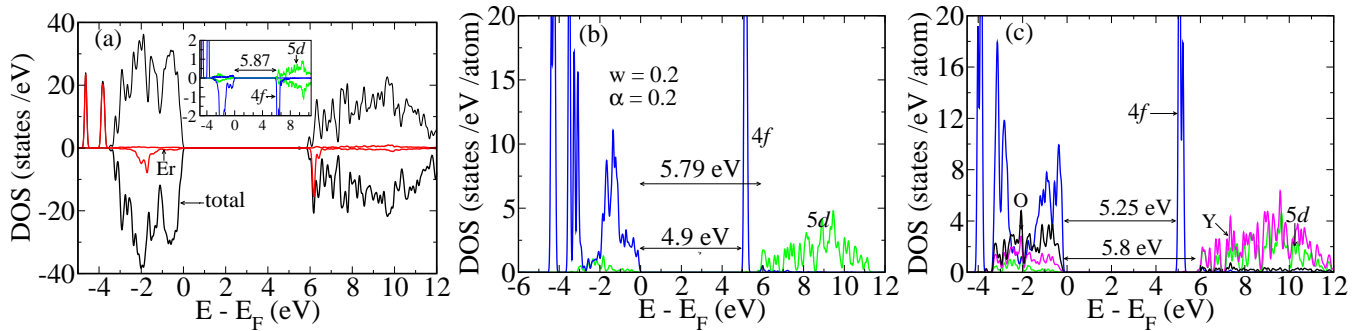


FIG. 6. (a) Spin-polarized total DOS *in black* and Er PDOS *in red* of Er-substituted  $\text{Y}_2\text{O}_3$  in  $C_{3i}$ -site and HSE06, and (b) Er PDOS computed with HSE and SOC with  $\alpha = 0.2$   $w = 0.2$  and (c) HSE06,  $U$  ( $U_{eff} = -2$  eV), and SOC. The positive and negative values represent the DOS for spin-up and spin-down electrons. The inset in (a) shows the partial density of states of Er 5d in green and 4f in blue. The band gap as well as the 4f-5d splittings slightly change depending the choice of the HSE parameters.

ment with experiment. The tuned HSE with  $\alpha = 0.2$  and  $w = 0.2 \text{ \AA}^{-1}$  slightly reduces the band gap and 4f splittings. As expected, reducing the exact short-range Hartree-Fock exchange  $E_x^{HF,SR}$  reduces the 4f-4f splittings. The 4f-5d excitation energy is now much closer to experiment. In addition, it also leads to a slight decrease in the band gap for the host.

The third set of calculations above, (iii), have a negative  $U_{eff} = -2$  eV, which is theoretically possible when the exchange term  $J$  is larger than the on-site Coulomb term<sup>54–56</sup>  $U$ , especially for *sp*-like delocalized states. Now, as expected, this approach further reduces the 4f-4f splittings due to the negative value of  $U_{eff}$ , whereas the 4f to 5d excitation energy remains more or less the same. Overall the HSE results obtained with different parameters are very similar qualitatively. Further fine tuning of these parameters and their validation requires additional experimental data.

## VI. CONCLUSION

By performing DFT calculations, we investigated the dopant formation energy and the electronic structure of Er doped yttria in order to assess the utility of the material for quantum devices such as quantum memories and quantum transducers. Our results indicate that neutral Er is lower energy in the  $C_2$  site relative to the  $C_{3i}$  site, which may enable controlled preferential positioning of Er in that specific site during growth. The formation energy calculations show that the charge-neutral Er dopant is more stable than charged Er dopants. The electronic structure obtained with PBE +  $U$  calculations reveals the orbital ( $\sim 6 \mu_B$ ) and spin ( $\sim 3 \mu_B$ ) magnetic moments, and the occupancy (11 electrons) of Er 4f, confirming the formation of  $\text{Er}^{3+}$ .

We computed the first and second electronic excitation energies using a minimal atomistic model, incorporating the first-principles calculated spin-orbit parameter, and these excitation energies agree well with photolumines-

cence data. Since our  $U$  only is for the *d* and *f* states, and the highest valence and lowest conduction states are neither *d* nor *f*, within standard DFT the inclusion of  $U$  and SOC does not change the band gap of the host. A more advanced approach using a standard HSE functional produces more robust electronic band features viz., the host band gap and the alignment of the Er 4f and 5d states, which remain more or less the same even with a small variation of HSE parameters and  $U$ .

Even in material with Er at both  $C_2$  and  $C_{3i}$  sites, the site energy preference has important implications for spin-photon interfaces. The  $C_{3i}$  sites could be depleted of one electron by co-doping with electron acceptors or through a gate voltage. At the temperatures relevant for quantum devices ( $< 1$  K) this would yield a material with only the Er in  $C_2$  sites that have the optical transitions associated with  $\text{Er}^{3+}$ . Such a material would be preferred for the quantum memories that benefit from a static electric dipole that permits shifting the optical transition energy into or out of resonance with an optical cavity. If the erbium-doped yttria is to be used for quantum transduction then the material should be co-doped with electron donors, or a gate voltage used, to ensure all the Er  $C_{3i}$  sites are neutral. Furthermore the use of a gate voltage can permit the shift of the  $C_2$  site optical transitions far away from the narrow linewidth optical band associated with the  $C_{3i}$  sites and thus optimizing the material for quantum transduction. We conclude that yttria is a remarkable material whose spin-photon interfaces may be optimized for performance either as quantum memories or quantum transducers.

## ACKNOWLEDGMENTS

Work done at the Ames Laboratory was conducted for the US-DOE under its contract with Iowa State University, Contract No. DE-AC02-07CH11358. MEF acknowledges support from NSF DMREF DMR-1921877 for studies of the difference in formation energies be-

tween the  $C_2$  and  $C_{3i}$  sites. Atomistic simulation of the excitation energies, as well as hybrid functional calculations of the band gap and partial densities of states were supported by the U. S. Department of Energy, Office of

Science, Office of Basic Energy Sciences, under Award Number DE-SC0023393. We acknowledge fruitful conversations with Tian Zhong.

- \* These two authors contributed equally.
- <sup>1</sup> P. Goldner, A. Ferrier, and O. Guillot-Noel, *Handbook on the Physics and Chemistry of Rare Earths* **46**, 1 (2015).
  - <sup>2</sup> B. Jacquier *et al.*, *Spectroscopic properties of rare earths in optical materials*, Vol. 83 (Springer Science & Business Media, 2005).
  - <sup>3</sup> D. P. DiVincenzo, *Fortschritte der Physik* **48**, 771 (2000).
  - <sup>4</sup> M. V. G. Dutt, L. Childress, L. Jiang, E. Togan, J. Maze, F. Jelezko, A. S. Zibrov, P. R. Hemmer, and M. D. Lukin, *Science* **316**, 1312 (2007).
  - <sup>5</sup> C. Yin, M. Rancic, G. G. de Boo, N. Stavrias, J. C. McCalmum, M. J. Sellars, and S. Rogge, *Nature* **497**, 91 (2013).
  - <sup>6</sup> T. Kornher, D.-W. Xiao, K. Xia, F. Sardi, N. Zhao, R. Kolesov, and J. Wrachtrup, *Phys. Rev. Lett.* **124**, 170402 (2020).
  - <sup>7</sup> B. Hensen, H. Bernien, A. E. Dréau, A. Reiserer, N. Kalb, M. S. Blok, J. Ruitenbergh, R. F. L. Vermeulen, R. N. Schouten, C. Abellán, W. Amaya, V. Pruneri, M. W. Mitchell, M. Markham, D. J. Twitchen, D. Elkouss, S. Wehner, T. H. Taminiou, and R. Hanson, *Nature* **526**, 682 (2015).
  - <sup>8</sup> W. Tittel, M. Afzelius, T. Chanelière, R. Cone, S. Kröll, S. Moiseev, and M. Sellars, *Laser & Photonics Reviews* **4**, 244 (2010).
  - <sup>9</sup> T. Zhong, J. M. Kindem, J. G. Bartholomew, J. Rochman, I. Craiciu, V. Verma, S. W. Nam, F. Marsili, M. D. Shaw, A. D. Beyer, and A. Faraon, *Phys. Rev. Lett.* **121**, 183603 (2018).
  - <sup>10</sup> P. Siyushev, K. Xia, R. Reuter, M. Jamali, N. Zhao, N. Yang, C. Duan, N. Kukharchyk, A. D. Wieck, R. Kolesov, and J. Wrachtrup, *Nature Communications* **5**, 3895 (2014).
  - <sup>11</sup> H. Wang, M. Uehara, H. Nakamura, M. Miyazaki, and H. Maeda, *Advanced Materials* **17**, 2506 (2005).
  - <sup>12</sup> F. Vetrone, J.-C. Boyer, J. A. Capobianco, A. Speghini, and M. Bettinelli, *Journal of Applied Physics* **96**, 661 (2004).
  - <sup>13</sup> R. Muenchausen, L. Jacobsohn, B. Bennett, E. McKigney, J. Smith, J. Valdez, and D. Cooke, *Journal of Luminescence* **126**, 838 (2007).
  - <sup>14</sup> G. K. Das and T. T. Y. Tan, *The Journal of Physical Chemistry C* **112**, 11211 (2008).
  - <sup>15</sup> Y. Mao, T. Tran, X. Guo, J. Y. Huang, C. K. Shih, K. L. Wang, and J. P. Chang, *Advanced Functional Materials* **19**, 748 (2009).
  - <sup>16</sup> M. Dammak, R. Maalej, M. Kamoun, and J.-L. Deschannes, *physica status solidi (b)* **239**, 193 (2003).
  - <sup>17</sup> M. K. Singh, A. Prakash, G. Wolfowicz, J. Wen, Y. Huang, T. Rajh, D. D. Awschalom, T. Zhong, and S. Guha, *APL Materials* **8**, 031111 (2020).
  - <sup>18</sup> M. Scarafagio, A. Tallaire, K.-J. Tielrooij, D. Cano, A. Grishin, M.-H. Chavanne, F. H. L. Koppens, A. Ringuedé, M. Cassir, D. Serrano, P. Goldner, and A. Ferrier, *The Journal of Physical Chemistry C* **123**, 13354 (2019).
  - <sup>19</sup> J. B. Gruber, R. P. Leavitt, C. A. Morrison, and N. C. Chang, *The Journal of Chemical Physics* **82**, 5373 (1985).
  - <sup>20</sup> Klintonberg, S. Edvardsson, and J. Thomas, *Journal of Alloys and Compounds* **275-277**, 174 (1998).
  - <sup>21</sup> K. I. Portnoi, N. I. Timofeeva, S. E. Salibekov, and I. V. Romanovich, *Chemischer Informationsdienst* **3**, 0009 (1972).
  - <sup>22</sup> G. Kresse and J. Furthmüller, *Phys. Rev. B* **54**, 11169 (1996).
  - <sup>23</sup> S. L. Dudarev, G. A. Botton, S. Y. Savrasov, C. J. Humphreys, and A. P. Sutton, *Phys. Rev. B* **57**, 1505 (1998).
  - <sup>24</sup> D. Hobbs, G. Kresse, and J. Hafner, *Phys. Rev. B* **62**, 11556 (2000).
  - <sup>25</sup> G. Kresse and J. Furthmüller, *Computational Materials Science* **6**, 15 (1996).
  - <sup>26</sup> G. Kresse and D. Joubert, *Phys. Rev. B* **59**, 1758 (1999).
  - <sup>27</sup> P. Giannozzi, S. Baroni, N. Bonini, M. Calandra, R. Car, C. Cavazzoni, D. Ceresoli, G. L. Chiarotti, M. Cococcioni, I. Dabo, *et al.*, *Journal of Physics: Condensed matter* **21**, 395502 (2009).
  - <sup>28</sup> P. Giannozzi, O. Andreussi, T. Brumme, O. Bunau, M. B. Nardelli, M. Calandra, R. Car, C. Cavazzoni, D. Ceresoli, M. Cococcioni, N. Colonna, I. Carnimeo, A. D. Corso, S. de Gironcoli, P. Delugas, R. A. DiStasio, A. Ferretti, A. Floris, G. Fratesi, G. Fugallo, R. Gebauer, U. Gerstmann, F. Giustino, T. Gorni, J. Jia, M. Kawamura, H.-Y. Ko, A. Kokalj, E. Küçükbenli, M. Lazzeri, M. Marsili, N. Marzari, F. Mauri, N. L. Nguyen, H.-V. Nguyen, A. O. de-la Roza, L. Paulatto, S. Poncé, D. Rocca, R. Sabatini, B. Santra, M. Schlipf, A. P. Seitsonen, A. Smogunov, I. Timrov, T. Thonhauser, P. Umari, N. Vast, X. Wu, and S. Baroni, *Journal of Physics: Condensed Matter* **29**, 465901 (2017).
  - <sup>29</sup> E. N. Brothers, A. F. Izmaylov, J. O. Normand, V. Barone, and G. E. Scuseria, *The Journal of Chemical Physics* **129**, 011102 (2008).
  - <sup>30</sup> J. Heyd, G. E. Scuseria, and M. Ernzerhof, *The Journal of Chemical Physics* **124**, 219906 (2006).
  - <sup>31</sup> J. Jalli, Y.-K. Hong, S.-H. Gee, S. Bae, J. Lee, J. C. Sur, G. S. Abo, A. Lyle, S.-I. Lee, H. Lee, and T. Mewes, *IEEE Transactions on Magnetics* **44**, 2978 (2008).
  - <sup>32</sup> F. Hanic, M. Hartmanová, G. G. Knab, A. A. Urusovskaya, and K. S. Bagdasarov, *Acta Crystallographica Section B* **40**, 76 (1984).
  - <sup>33</sup> H. A. Badehian, H. Salehi, and M. Ghoohestani, *Journal of the American Ceramic Society* **96**, 1832 (2013).
  - <sup>34</sup> S. B. Zhang and J. E. Northrup, *Phys. Rev. Lett.* **67**, 2339 (1991).
  - <sup>35</sup> G. Makov and M. C. Payne, *Phys. Rev. B* **51**, 4014 (1995).
  - <sup>36</sup> C. Freysoldt, J. Neugebauer, and C. G. Van de Walle, *Phys. Rev. Lett.* **102**, 016402 (2009).
  - <sup>37</sup> C. Freysoldt, J. Neugebauer, and C. G. Van de Walle, *physica status solidi (b)* **248**, 1067 (2011).



- <sup>38</sup> M. Gurvitch, L. Manchanda, and J. M. Gibson, *Applied Physics Letters* **51**, 919 (1987).
- <sup>39</sup> R. A. Robie, B. S. Hemingway, and J. R. Fisher, *Thermodynamic properties of minerals and related substances at 298.15 K and 1 bar (10<sup>5</sup> pascals) pressure and at higher temperatures*, Tech. Rep. (Geological Survey, Washington, DC (USA), 1978).
- <sup>40</sup> T. T. Van, J. R. Bargar, and J. P. Chang, *Journal of Applied Physics* **100**, 023115 (2006).
- <sup>41</sup> S. Hfner, *Advances in Physics* **43**, 183 (1994).
- <sup>42</sup> M. Ramzan, Y. Li, R. Chimata, and R. Ahuja, *Computational Materials Science* **71**, 19 (2013).
- <sup>43</sup> Y.-N. Xu, Z.-Q. Gu, and W. Y. Ching, *Phys. Rev. B* **56**, 14993 (1997).
- <sup>44</sup> D. R. Mueller, D. L. Ederer, J. van Ek, W. L. O'Brien, Q. Y. Dong, J. Jia, and T. A. Callcott, *Phys. Rev. B* **54**, 15034 (1996).
- <sup>45</sup> T. Tomiki, J. Tamashiro, Y. Tanahara, A. Yamada, H. Fukutani, T. Miyahara, H. Kato, S. Shin, and M. Ishigame, *Journal of the Physical Society of Japan* **55**, 4543 (1986).
- <sup>46</sup> S. Zhang and R. Xiao, *Journal of Applied Physics* **83**, 3842 (1998).
- <sup>47</sup> R. Ahlawat, *Advanced Materials Proceedings* **2**, 687 (2017).
- <sup>48</sup> W. Y. Ching and Y.-N. Xu, *Phys. Rev. Lett.* **65**, 895 (1990).
- <sup>49</sup> V. I. Anisimov, F. Aryasetiawan, and A. I. Lichtenstein, **9**, 767 (1997).
- <sup>50</sup> J. Jensen and A. R. Mackintosh, Clarendon Press, Oxford (1991).
- <sup>51</sup> F. Viñes, O. Lamiel-García, K. Chul Ko, J. Yong Lee, and F. Illas, *Journal of Computational Chemistry* **38**, 781 (2017).
- <sup>52</sup> M.-A. Haa and A. N. Alexandrova, *Journal of Chemical Theory and Computation* **12**, 2889 (2016), pMID: 27163165.
- <sup>53</sup> A. Janotti, J. B. Varley, P. Rinke, N. Umezawa, G. Kresse, and C. G. Van de Walle, *Phys. Rev. B* **81**, 085212 (2010).
- <sup>54</sup> R. Micnas, J. Ranninger, and S. Robaszkiewicz, *Rev. Mod. Phys.* **62**, 113 (1990).
- <sup>55</sup> H. Nakamura, N. Hayashi, N. Nakai, M. Okumura, and M. Machida, *Physica C: Superconductivity* **469**, 908 (2009), proceedings of the 21st International Symposium on Superconductivity (ISS 2008).
- <sup>56</sup> I. Hase and T. Yanagisawa, *Phys. Rev. B* **76**, 174103 (2007).